

Filopodia were evident as early as the first observation time point (about 10 min) and persisted for 2 to 4 hours, after which period they became less evident as the spreading cell perimeter extended to encompass them. In both control cell lines and those expressing GAP-43, the cell perimeter often exhibited broad, thin, ruffled lamellipodia (Fig. 3).

Process formation from four independent cell lines transfected with a control plasmid and four independent lines expressing the highest amounts of GAP-43 was determined. All four GAP-43 lines expressed similar levels of GAP-43 by protein blot analysis. All CHO cell lines expressing GAP-43 had a greater tendency to extend processes than did control cell lines (Fig. 4). Whereas 14 to 40% of cells expressing GAP-43 had processes longer than 20 μm , only 3 to 5% of control cells had processes of this length. In addition, 6 to 11% of cells expressing GAP-43 had multiple processes and only 0.5 to 1% of control cells showed this feature. The lengths of the processes in cells expressing GAP-43 also exceeded those in control cells.

One interpretation of our data is that GAP-43 contributes a uniquely neuronal structure to these non-neuronal cells. A more likely explanation, however, is that GAP-43 interacts with general mechanisms that control cell shape (12) and thereby enhances filopodial extension. Many cells can extend filopodia or lamellipodia, depending upon several factors, including the phase of the cell cycle, plating conditions, and second messenger concentrations (13). Thus, although cells that have GAP-43 tend to have more filopodia, this does not prove that GAP-43 plays an identical role in neurons. Such a role does not seem unreasonable however, given that the movement of growth cones is likely mediated by mechanisms such as cortical actin flow and selective adhesion, which are general means to impart cellular motion (12).

It has been inferred from the localization and regulation of GAP-43 that this protein is important to nerve terminal plasticity. Our results are consistent with a model whereby GAP-43 controls the dynamics of the nerve terminal membrane structure during growth. This system additionally provides a bioassay that may be used to dissect functional regions of GAP-43 and to determine how the protein may interact with second messengers and the cytoskeleton to cause this particular membrane activity.

REFERENCES AND NOTES

1. J. H. P. Skene and M. Willard, *J. Cell Biol.* **89**, 86 (1981); *ibid.*, p. 96; L. I. Benowitz, V. E. Shashoua, M. G. Yoon, *J. Neurosci.* **1**, 300 (1981); K. F.

- Meiri, M. Willard, M. I. Johnson, *ibid.* **8**, 2571 (1988); GAP-43 is also known as B-50, F1, pp46, and P-57. For reviews see L. I. Benowitz and A. Routtenberg [*Trends Neurosci.* **10**, 527 (1987)] and M. C. Fishman [in *Assembly of the Nervous System*, L. Landmesser, Ed. (Liss, New York, in press)].
2. H. F. Federoff, E. Graczyk, M. C. Fishman, *J. Biol. Chem.* **263**, 19290 (1988).
3. F. Katz, L. Ellis, K. H. Pfenninger, *J. Neurosci.* **5**, 1402 (1985); P. N. E. DeGraan *et al.*, *Neurosci. Lett.* **61**, 235 (1985); K. F. Meiri, K. H. Pfenninger, M. B. Willard, *Proc. Natl. Acad. Sci. U.S.A.* **83**, 3537 (1986); J. H. P. Skene *et al.*, *Science* **233**, 783 (1986).
4. A. Rosenthal *et al.*, *EMBO J.* **6**, 3641 (1987); L. I. Benowitz, P. J. Apostolides, N. Perrone-Bozzozero, S. P. Finklestein, H. Zwiers, *J. Neurosci.* **8**, 339 (1988); R. L. Neve, E. A. Finch, E. D. Bird, L. I. Benowitz, *Proc. Natl. Acad. Sci. U.S.A.* **85**, 3638 (1988); S.-C. Ng, S. M. de la Monte, G. L. Conboy, L. R. Karns, M. C. Fishman, *Neuron* **1**, 133 (1988).
5. S. M. de la Monte, H. F. Federoff, S.-C. Ng, E. Graczyk, M. C. Fishman, *Dev. Brain Res.*, in press.
6. R. F. Akers and A. Routtenberg, *J. Neurosci.* **7**, 3976 (1987).
7. K. A. Alexander, B. T. Wakim, G. S. Doyle, K. A. Walsh, D. R. Storm, *J. Biol. Chem.* **263**, 7544 (1988); T. J. Andreasen, C. W. Luetje, W. Heide-man, D. R. Storm, *Biochemistry* **22**, 4615 (1983).
8. C. O. M. Van Hoof, P. N. E. De Graan, A. B. Oestreicher, W. H. Gispen, *J. Neurosci.* **8**, 1789 (1988).
9. B. Seed and A. Aruffo, *Proc. Natl. Acad. Sci. U.S.A.* **84**, 3365 (1987).
10. Y. Gluzman, *Cell* **23**, 175 (1981).
11. G. Della-Valle, R. Fenton, C. Basilico, *Mol. Cell. Biol.* **1**, 418 (1981).
12. D. Bray and J. G. White, *Science* **239**, 883 (1988); S. J. Smith, *ibid.* **242**, 708 (1988); J. P. Trinkuns, in *Biology of the Nerve Growth Cone*, S. Kater and P. Letourneau, Eds. (Liss, New York, 1988), pp. 1–19.
13. L. E. Allred and K. R. Porter in *Surfaces of Normal and Malignant Cells*, R. O. Hynes, Ed. (Wiley, New York, 1979), pp. 21–32.
14. L. R. Karns, S.-C. Ng, J. A. Freeman, M. C. Fishman, *Science* **236**, 597 (1987).
15. B. Seed, *Nature* **329**, 840 (1987).
16. ——— and A. Aruffo, personal communications.
17. M. X. Zuber, E. R. Simpson, M. R. Waterman, *Science* **234**, 1258 (1986).
18. K. Van-Doren, D. Hanahan, Y. Gluzman, *J. Virol.* **50**, 607 (1984).
19. F. M. Ausubel *et al.*, Eds., *Current Protocols in Molecular Biology* (Green Publishing Associates/Wiley-Interscience, New York, 1987), vol. 1, pp. 9.0.1–9.5.6.
20. We thank B. Seed for the plasmid pCDM8, C. Basilico for the WOP cells, and J. Jackson for preparation of the manuscript. M.X.Z. is the recipient of a postdoctoral fellowship from the American Cancer Society and D.W.G. has partial support from an Institutional Physician Scientist Award from NIH.

18 November 1988; accepted 8 March 1989

Three-Dimensional Structure of Human Serum Albumin

DANIEL C. CARTER,* XIAO-MIN HE, SIBYL H. MUNSON, PAMELA D. TWIGG, KIM M. GERNERT, M. BETH BROOM, TERESA Y. MILLER

The three-dimensional structure of human serum albumin has been solved at 6.0 angstrom (\AA) resolution by the method of multiple isomorphous replacement. Crystals were grown from solutions of polyethylene glycol in the infrequently observed space group $P4_212$ (unit cell constants $a = b = 186.5 \pm 0.5 \text{ \AA}$ and $c = 81.0 \pm 0.5 \text{ \AA}$) and diffracted x-rays to lattice d -spacings of less than 2.9 \AA . The electron density maps are of high quality and revealed the structure as a predominantly α -helical globin protein in which the course of the polypeptide can be traced. The binding loci of several organic compounds have been determined.

THE SERUM ALBUMIN PROTEINS ARE among the most highly studied and applied in biochemistry (1–4). These proteins possess high helical content and high cysteine content (17 disulfides), and have approximate molecular weights of 65 kD. Human serum albumin (HSA) comprises 585 amino acids with a molecular weight of 66,500 daltons. Complete amino acid sequences are known for HSA (5) and for bovine and rat serum albumins (6, 7). Comparisons of these amino acid sequences reveal high sequence homology. The serum albumins also possess internal sequence homology in the form of three tandem gene duplications (hereafter referred to as domains I, II, and III). In addition to three tandem gene duplications, there may be as

many as six repeating structural motifs based on the position and frequency of the exon junctures (8). Although the principal function of serum albumin remains disputed, as the most abundant plasma protein of the circulatory system it contributes significantly to colloidal osmotic blood pressure and to many transport and regulatory processes. A number of studies have focused on the multifunctional binding properties of serum albumin. This protein binds a wide variety of substrates, ranging from metals such as calcium and copper to fatty acids, amino

National Aeronautics and Space Administration, Space Sciences Laboratory, Code ES76 Biophysics Branch, Marshall Space Flight Center, AL 35812.

*To whom correspondence should be addressed.

acids, hormones, and an impressive spectrum of therapeutic drugs. The majority of these drug-binding studies involving HSA have shown that the distribution, free concentration, and metabolism of various pharmaceuticals can be significantly altered as a function of their binding constant to HSA.

A detailed knowledge of the three-dimensional (3-D) structure of serum albumin is imperative in order to understand fully the binding modes, as well as many of the physical properties, of this protein. In addition, since many pharmaceuticals are rendered less effective or entirely ineffective by virtue of their interaction with HSA, it is apparent that the crystal structure of serum albumin, particularly the human form, should find broad and significant application in the area of rational drug design. The structure of serum albumin has been the goal of crystallographic investigations for many years and although several crystal forms have been obtained (9, 10), previous efforts to determine the 3-D structure of

serum albumin have been unrewarding. We report the structure determination of HSA based on a new tetragonal crystal form.

We produced crystals from commercial preparations of fatty-acid-free recrystallized fraction V HSA after the work of Cohn *et al.* (11) and Chen (12). Protein that was further purified by a variety of methods, including fast protein liquid chromatography, also produced crystals, but with no observed improvement of crystal quality. Crystals of HSA were grown from polyethylene glycol (PEG) by the standard hanging-drop technique with the use of Linbro plates (13). Solutions of 120 to 180 mg per milliliter of HSA (5 μ l) were added to precipitant solutions of 40% PEG 400 in 0.05M KH_2PO_4 , adjusted to pH 6.8 (5 μ l), and inverted and sealed over 1-ml reservoirs containing the same precipitant solution (14). Although crystals used in the structure determination were typically grown at 20°C, crystals grew within a pH range of 5.5 to 7.2 and temperatures from 4° to 28°C. The crystals appeared in 24 to 48 hours as tetragonal plates and reached 0.5 to 2.0 mm in size in 3 to 10 days.

X-ray precession photographs of the crystals indicate $4mm$ symmetry for the $hk0$ zone (Fig. 1A) and mm symmetry for the hhl , $h0l$, and $0kl$ zones. Thus the Laue symmetry is $4/mmm$. The $h00$ and $0k0$ zones show systematic absences for h or $k = 2n + 1$. As there are no systematic absences along the $00l$ direction, the space group is the infrequently observed $P4_21_2$. Consistent with the presence of an isotropic axis, the crystals do not extinguish polarized light when viewed

down the fourfold axis. The unit cell constants are $a = b = 186.5 \pm 0.5 \text{ \AA}$ and $c = 81.0 \pm 0.5 \text{ \AA}$. Calculation of Matthews' coefficients, based on the unit cell constants, a molecular weight of 66,500, and a partial specific volume for HSA of $0.733 \text{ cm}^3/\text{g}$, suggests solvent contents of 77 or 55% based upon one and two molecules in the asymmetric unit, respectively (15). Oscillation photographs taken at Brookhaven Synchrotron Light Source (BNLS) show diffraction to lattice d -spacings of 3.0 \AA by visual inspection (Fig. 1B). Native data collected on a multiwire x-ray area detector show integrated intensities to d -spacings of less than 2.9 \AA . The structure of HSA was determined by multiple isomorphous replacement (MIR) (16, 17). The first successfully recognized derivative, prepared from HgCl_2 , produced a striking difference Patterson map. The signal of this Patterson map was greatly enhanced because of the fortuitous occurrence that the sum of the fractional coordinates of the Hg atom, X and Y , approximately equaled 0.5, which caused many of the heavy atom vectors to overlap. The interpretation indicated a single-site derivative consistent with an Hg atom reacting with the single free sulfhydryl of HSA near the NH_2 -terminus (Cys^{34}). This derivative provided initial protein phases by the method of single isomorphous replacement and solvent flattening (18). These phases were of adequate quality to reveal the gross molecular packing in the crystal, but insufficient to reveal any molecular details. Difference Fourier maps produced by these phases eventually aided in the interpretation of

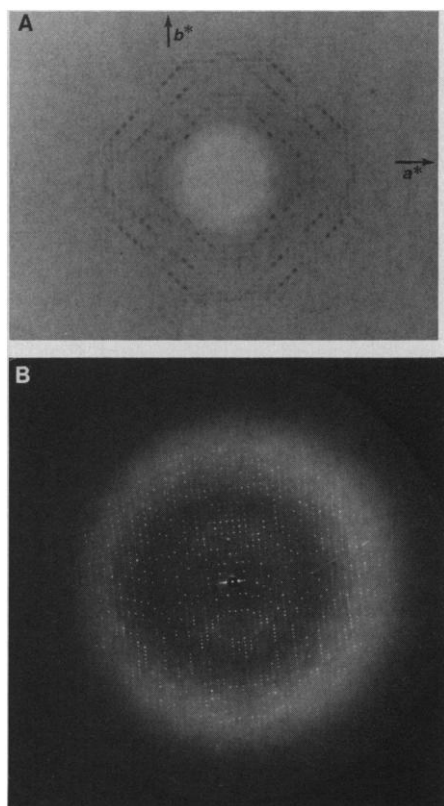


Fig. 1. (A) An enlarged section of an $hk0$ precession photograph of HSA illustrating the presence of a low-resolution superlattice phenomenon with cell constants of $a' = b' = 132 \text{ \AA}$ in the $hh0$ direction. (B) A 0.5° oscillation photograph of a tetragonal HSA crystal taken at BNLS (beamline conditions: 2.5 GeV and 60 mA, $CF = 107 \text{ mm}$, and $\lambda = 1.22 \text{ \AA}$). The crystal is misset slightly from the a -axis. This crystal shows diffraction to lattice d -spacings of 3.0 \AA . The resolution limit of the photograph corresponds to 2.4 \AA .

Table 1. Summary of crystallographic data. X-ray diffraction data were collected on a Siemens (Nicolet) area detector equipped with a helium path, operating on a Rigaku RU200 rotating anode x-ray generator with monochromated Cu K- α radiation. Diffraction data were processed with the Xengen data-reduction package (20). Crystals used for the heavy atom surveys were transferred to stabilizing solutions of 35 to 45% PEG 400 MW (phosphate or cacodylate buffer, pH 6.8 to 7.2), which included heavy atom reagents prepared according to standard procedures. Sixteen derivative data sets were used out of the more than 60 sets collected. The centric R -factors (R_c) for these 16 sets ranged from 0.56 to 0.74. Thermal parameters were fixed and not refined. Only three data sets with the best R_c values are shown. Native data were collected and merged from three crystals. Data processed consist of 14,529 observations (6% rejected) of 3,722 unique reflections to a resolution of 6.0 \AA with $R_{\text{sym}}(I) = 7.7\%$. Parameters = R_f , agreement between native and derivative structure factors; N , number of reflections; and D , resolution. [Coordinates submitted to the Brookhaven Protein Data Bank.]

Data set	Occu-pancy	X	Y	Z	R_c	R_f	N	D (\AA)
HSAH7A HgCl_2	1.000	0.4530	0.0538	0.2118	0.576	0.24	2105	6.8
	0.315	0.0830	0.4417	0.3636				
	0.219	0.1302	0.3469	0.3550				
HSAH12A HgI_2	1.000	0.2834	0.1908	0.0689	0.560	0.21	2191	6.0
	0.815	0.3760	0.0911	0.1414				
	0.534	0.3586	0.1613	0.0645				
HSA2ClA*	1.000	0.1282	0.3970	0.0793	0.660	0.15	3912	5.0
	0.857	0.0931	0.3530	0.1501				
	0.662	0.2814	0.1993	0.0512				
	0.550	0.4717	0.1009	0.3314				
	0.165	0.3795	-0.0014	0.2075				

*2-Chloromercuri-4-nitrophenol.

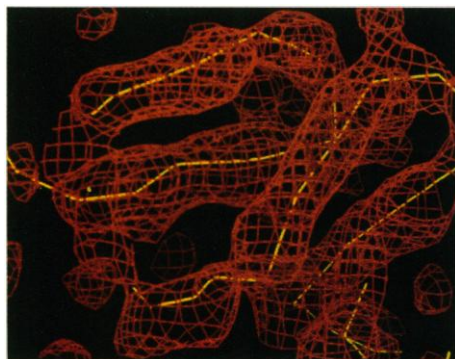


Fig. 2. Section of the electron density of subdomain IIB. The connectivity of the electron density based on coordinates obtained from the minimap and adjusted with the program FRODO is illustrated.



Fig. 3. Illustration of the molecular configuration of HSA based on the interpretation of the 6.0 Å electron density. The high degree of primary and tertiary structural homology between domains I, II, and III provided a useful cross-check of the topology. The binding sites within subdomains IA and IIIA are represented by red spheres. The overall molecular length is 137 Å. [This graphical representation of HSA was produced by the program SPHERES written by M. Carson.]

other derivatives. MIR phases based on these derivatives were subjected to phase refinement by solvent flattening and were used to determine the positions of minor sites, further allowing for the interpretation of several additional heavy-atom derivatives of lower occupancy. All major heavy atom positions determined with cross-phased Fourier maps were verified by consistency with the respective difference Patterson functions. The heavy atom parameters for each derivative were refined by least squares against the centric data. The phase distributions for each derivative were then calculated separately, cast into Hendrickson-Lattman formulation, and summed together (19). Currently, nine heavy atom derivatives suitable for the structure determination have been identified. The final phase set was produced from the nine derivatives through the phase combination of 16 individual data sets. This process resulted in MIR phases with a mean figure of merit (m) of 0.68 for 3210 reflections greater than 5σ at 6.0 Å resolution (Table 1). Several cycles of solvent flattening produced a final (m) of 0.80

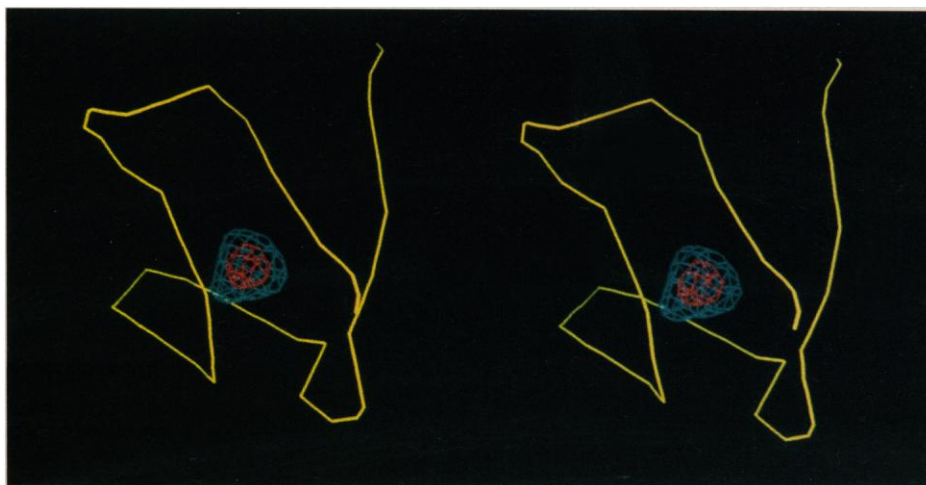


Fig. 4. Stereoview representing the flow of the polypeptide backbone in subdomain IA. The salicylic acid (aspirin) binding site is illustrated by the electron density $(F_{\text{complex}} - F_{\text{protein}})\alpha$ for 2522 reflections to 6.0 Å, where the phases, α , are from MIR followed by solvent flattening. Aspirin binds equally well within both subdomains IA and IIIA; however, many compounds, such as the diazepam, have a higher degree of affinity for IIIA. [This figure was produced by the program FRODO written by A. Jones (23).]

and a map inversion crystallographic R -factor of 0.35. This phase set was used to calculate the 6.0 Å electron density map.

An unusual feature of the electron density in this crystal structure is the occurrence of large solvent channels that run the length of the crystal and that are centered on the twofold axes parallel to the c axis (see cover). These solvent channels have cross sections of nearly 90 Å by 90 Å and produce an electron density pattern in agreement with the observation of a low-resolution superlattice phenomenon in the $hk0$ precession photograph (Fig. 1A). Initially, a lower estimate of 50% for the solvent content was used in the solvent-flattening and phase-recombination process. Further inspection of the MIR-phased electron density revealed a higher solvent content of 77% in this crystal form, indicating the presence of one molecule in the asymmetric unit. Thereafter, a conservative estimate of 72% for the solvent content was used in the solvent-flattening and phase-recombination processes. Prominent features of the electron density are winding coils 6 to 8 Å in diameter, indicative of α helix at this resolution (21). Aggregates of helices in this structure exhibit a right-handed twist, which suggests that the alternate enantiomorph is the correct choice (22). Determination of the absolute configuration of the structure with the use of anomalous scattering effects has been unsuccessful because of the lack of reliable signal at this resolution. The determination of the handedness of this structure requires higher resolution. This high percentage of helical structure agrees well with secondary-structure predictions (4). Despite the low resolution of the current phases and the potential com-

plexity of the HSA structure due to the presence of 17 disulfide bridges, the electron density at 6.0 Å reveals the course of virtually the entire polypeptide chain (Fig. 2). The initial chain tracing of the structure was based on interpretation of the electron density from minimaps. Further details of the electron density and cross-checks of the topology of each domain were examined with a Silicon Graphics Personal Iris and the program FRODO (23).

The overall molecular configuration of HSA is illustrated in Fig. 3. The high quality of information in the electron density map at 6.0 Å resolution, although unusual, is not unprecedented for largely α -helical proteins (21, 24). Nevertheless, the preliminary tracing for the entire polypeptide chain must be confirmed at a higher resolution stage. The molecular envelope for the protein is in excellent agreement with a variety of previous studies ranging from electro-hydrodynamic to low-angle x-ray scattering, which have depicted the serum albumins to be oblate ellipsoids with axes of 140 Å by 40 Å (25). Domains I, II, and III are structurally homologous. Each is made up of two subdomains referred to as A and B, formed by three to four α helices linked together by a long section of α helix. Subdomains IA, IB, and IIA pack tightly together, forming an enlarged head for the molecule, whereas subdomains IIB, IIIA, and IIIB form the extended tail. The average length of the helices in each bundle is approximately 20 Å. Subdomains IA, IIA, and IIIA are slightly larger, each supplementing the three-helix bundle with additional loops or small helices. The presence of six subdomains (IA, IB, IIA, IIB, IIIA, and IIIB) is corroborated by

the frequency and position of six homologous exons (8). Based on the interpretation of the 6.0 Å electron density map, and the internal sequence homology, we found that the longer intersubdomain helices correlate well with the amino acid sequences 101 to 124, 289 to 316, and 487 to 514. Similarly, the connections between domains I and II and II and III are nonhelical segments that may correspond to residues 177 to 200 and 369 to 392, respectively. The presence of long, somewhat solvent-exposed intersubdomain helices provides a logical basis for the observed reversible expansion and contraction of serum albumin under varying conditions of pH (4).

Preliminary binding studies, including those of heavy atom reagents, reveal that the majority of the binding in HSA for a chemically diverse group of small molecules takes place within the subdomains IA and IIIA, which are separated by an intramolecular distance of 83 Å (Fig. 4). The additional electron density that supplements the subdomains IA, IIA, and IIIA appears to correspond to the smaller disulfide double loops in the amino acid sequence (residues 75 to 101, 265 to 289, and 461 to 487) and it contributes to the structural framework responsible for the exceptional binding properties of the serum albumin proteins. Unlike the bilin binding protein from *Pieris brassicae* (26), retinal binding protein (27), and others that bind lipids within a β barrel, the binding structure of HSA is similar to that of many α-helical proteins, such as cytochrome c' and myoglobin. In this re-

gard, HSA is known to bind the metabolized protoporphyrins hemin and hematin (28). The apparent lack of binding in the homologous subdomain IIA can be rationalized by conformational or steric differences produced by its close association with both subdomains IA and IB. The strong binding site within subdomain IIIA agrees well with amino acid residues implicated in the primary fatty acid binding site (29), which is commonly referred to as Site 2. Although HSA is structurally distinct from other proteins, each domain has structural similarities to calmodulin (30). Since nearly one-half of the plasma calcium is bound to HSA, it is interesting to speculate whether this similarity of structure also extends to the mode of calcium binding to HSA (31). Further characterization of substrate binding must await the determination of the structure to higher resolution.

REFERENCES AND NOTES

1. T. Peters, *Adv. Protein Chem.* **37**, 161 (1985).
2. A. Kragh-Hansen, *Pharmacol. Rev.* **33**, 17 (1981).
3. T. Peters, *Albumin: An Overview and Bibliography* (Miles Laboratory, Elkhart, IN, 1980).
4. J. F. Foster, in *Albumin Structure, Function, and Uses*, V. M. Rosenoer, M. Oratz, M. A. Rothschild, Eds. (Pergamon, Oxford, 1977), pp. 53–84.
5. A. Dugiaczyk, S. W. Law, O. E. Dennison, *Proc. Natl. Acad. Sci. U.S.A.* **79**, 71 (1982).
6. J. R. Brown and P. Shockley, in *Lipid-Protein Interactions*, P. Jost and O. H. Griffith, Eds. (Wiley, New York, 1982), vol. 1, pp 25–68.
7. T. D. Sargent, M. Yang, J. Bonner, *Proc. Natl. Acad. Sci. U.S.A.* **78**, 243 (1981).
8. P. P. Minghetti *et al.*, *J. Biol. Chem.* **261**, 6747 (1986).
9. R. J. McClure and B. M. Craven, *J. Mol. Biol.* **83**, 551 (1974).
10. S. N. Rao *et al.*, *J. Biol. Chem.* **251**, 3191 (1976).
11. E. J. Cohn *et al.*, *J. Am. Chem. Soc.* **68**, 459 (1946).
12. R. F. Chen, *Arch. Biochem. Biophys.* **160**, 106 (1974).
13. A. McPherson, *Preparation and Analysis of Protein Crystals* (Wiley, New York, 1982).
14. D. C. Carter, application made for U.S. Patent, NASA case no. MFS-28234-1.
15. B. W. Matthews, *J. Mol. Biol.* **33**, 491 (1968).
16. D. W. Green, V. M. Ingram, M. F. Perutz, *Proc. R. Soc. London Ser. A* **225**, 287 (1954).
17. C. Bokhoven, J. C. Schoone, J. M. Bijvoet, *Acta Crystallogr.* **4**, 275 (1951).
18. B. C. Wang, *Methods Enzymol.* **115**, 90 (1985).
19. W. A. Hendrickson and E. E. Lattman, *Acta Crystallogr.* **B26**, 136 (1970).
20. A. J. Howard *et al.*, *J. Appl. Crystallogr.* **20**, 383 (1987).
21. M. F. Perutz *et al.*, *Nature* **185**, 416 (1960).
22. M. G. Rossmann and P. Argos, *Annu. Rev. Biochem.* **50**, 497 (1981).
23. T. A. Jones, *J. Appl. Crystallogr.* **11**, 268 (1978).
24. W. A. Hendrickson *et al.*, *Proc. Natl. Acad. Sci. U.S.A.* **72**, 2160 (1975).
25. A. K. Wright and M. R. Thompson, *Biophys. J.* **15**, 137 (1975).
26. R. Huber *et al.*, *J. Mol. Biol.* **195**, 423 (1987).
27. M. Z. Papiz *et al.*, *Nature* **324**, 383 (1986).
28. P. A. Adams and M. C. Berman, *Biochem. J.* **191**, 95 (1980).
29. T. Peters, Jr., and R. C. Feldhoff, *Biochemistry* **14**, 3384 (1975).
30. S. Y. Babu *et al.*, *J. Mol. Biol.* **204**, 191 (1988).
31. N. Fogh-Anderson, *Clin. Chem.* **23**, 2122 (1977).
32. Supported by the Center Director's Discretionary Fund and the Office of Space Science and Applications of the National Aeronautics and Space Administration. X.-M.H., S.H.M., M.B.B., and P.D.T. were supported under contract with the Universities Space Research Association. We thank A. Howard for assistance with Xengen, M. Carson for graphics programs, W. Munson and J. Reynolds for helpful assistance with the manuscript, R. Sweet and P. Levine of the Brookhaven National Synchrotron Light Source for the generous use of their facilities and helpful assistance with the synchrotron experiments, and R. Snyder, V. Yost, T. Peters, F. Putnam, and M. F. Perutz for their constant interest and encouragement.

16 February 1989; accepted 26 April 1989